Indian Journal of Pure & Applied Physics
Vol. 64, October 2026, pp. 1075-1082
DOI: 10.56042/ijpap.v64i10.23809

Decolorization of Toxic Dyes using Biosynthesized Manganese Oxide Nanoparticles under Sun Light

Jagdish Arekar[a], Dipak J Garole[b], Yogesh R Toda[c] & Ratnamala S Bendre[a*]

[a]School of Chemical Sciences, North Maharashtra University, Maharashtra, 425 001, India

[b]Directorate of Geology and Mining, Government of Maharashtra, Maharashtra, 440 010, India

[c]Department of Science & Humanities, Nano Materials Research Lab, Government College of Engineering, Maharashtra, 425 001, India

Received: 15th September 2025; accepted: 1st September 2026

Manganese oxide nanoparticles (MnO_2-NPs) have been biosynthesized using the aqueous extract of the plant powder of Lagerstroemia speciosa. This plant contains steroids, terpenoids, glycosides, phenolic compounds, α-amino acids, saponins, starch, alkaloids, carbohydrates, organic acids, flavonoids, reducing sugars, and tannins. The phenolic compounds in the extract are exploited as reducing and capping agents. Biosynthesized particles have been characterized using UV-VIS-IR, XRD, FESEM, TGA, DSC, and FTIR analysis. The UV-Vis-IR spectrum clearly showed an absorption peak at 365 nm, which indicated the formation of MnO_2-NPs. It is evident in the FESEM images that the biosynthesized particles are rough, spherical, and arbitrarily oriented with a size of about 83–400 nm. The XRD analysis revealed a pure tetragonal structure for MnO_2-NPs with preferential orientation at (110) planes of reflection. Furthermore, the photocatalytic activity of MnO_2-NPs has been investigated by decolorizing methyl orange (MO) and bromocresol green (BCG) dyes under sunlight.

Keywords: MnO_2-NPs, UV-VIS-IR, XRD, FESEM, TGA, DSC, FTIR, Decolorization

1 Introduction

In nanotechnology, particle size plays a major function in forming a material. When nanoparticles are synthesized at the nanoscale, their unique optical, structural, and magnetic properties become particularly significant for researchers. The properties of nanoparticles are strongly influenced by several key parameters, including particle size, shape, crystal structure, and chemical composition[1].

Morphology and dimension are the controlling factors of the particle size of nanoparticles; thus, materials show stable characteristic properties. Therefore, nanoparticle synthesis depends on their core structure and controlled size[2, 3]. The fraction of atoms on the metal nanoparticles has a high specific surface area and is studied extensively because of their unique physical and electronic characteristics[4]. Excellent physicochemical properties of manganese oxide nanoparticles can be applied in various fields, as, catalysts, molecular sieves, batteries, and magnetic materials, as well as other applications such as water treatment, optoelectronics, etc[5]. Synthesized manganese oxide nanoparticles are studied for their optical and electronic properties and are the most prominent focusing elements for further research in solar cells[6]. Manganese oxide nanomaterials can be formed by various methods, such as the femtosecond laser ablation technique[7], reflux treatment method[8], redox method[9], green synthesis[10], the co-precipitation method[11], and the sol-gel process[12].

Recently, the biosynthetic route has been passed on as a proficient and fresh procedure for synthesizing nanomaterials. Typically, biosynthesis involves natural materials in the form of stems, seeds, roots, leaves, fruits, bark of plantsas well as various microbes like fungi, yeast, bacteria, etc. The precursor salts and particular metal ions are implicitly reduced by diverse, non-toxic, naturally accessible biomolecules like steroids, tannins, flavonoids, alkaloids, terpenes, saponins, etc[13-15]. Manganese oxide nanoparticles have raised the awareness of the majority of scientists because of their low cost and eco-responsiveness, which has established their expediency as a catalyst for organic dye deprivation, photocatalytic, biological, electrical, sensing, and optoelectronics applications due to their surface chemical activity and their physical characteristics. Most reports target the characterization and

*Corresponding author: E-mail: bendrers@rediffmail.com

application of the formed manganese nanoparticles in electronic properties. Still, the photocatalytic activity of MnO_2-NPs has been investigated seldom by performing the decolorization of methyl orange and bromocresol green dyes under sunlight.

Based on the above deliberations, this analysis deals with the synthesis of MnO_2 nanoparticles through the green method using the extract of leaves of Lagerstroemia speciosa. The work focuses mainly on decolorizing methyl orange and bromocresol green dyes under sunlight.

2.1 Preparation of Plant Extract

A small amount of big leaves from the *Lagerstroemia speciosa* plant were collected and washed thoroughly with water to eliminate any dirt or debris on the surface. Finely ground 5 g plant powder was extracted with 100 ml of Milli-Q water in a boiling water bath for 30 minutes and filtered with Whatmann No. 1 filter paper. The plant extract is stored and refrigerated at 6 °C before use.

2.2 Synthesis Method of Mn-NPs

Manganese acetate (1 mm) was a precursor to synthesize the Mn nanoparticles. A 0.1 M solution of this salt was prepared by adding 1.73 g of it to 100 ml of distilled water. To synthesize Mn-NPs, 100 ml of the above plant extract was added dropwise to the 100 ml of 0.1 M manganese acetate solution which is previously heated at 60 °C. After adding plant extract, the solution mixture was heated at 80 °C for 30 min. A color change (from colorless to dark brown or black) indicated the formation of Mn-NPs (Fig. 1). The solution was cooled down to room temperature. The resultant solution was centrifuged at 15000 rpm for 15 min, the supernatant solution was decanted, and the residue (Mn-NPs) was dried at 60 °C in an oven.

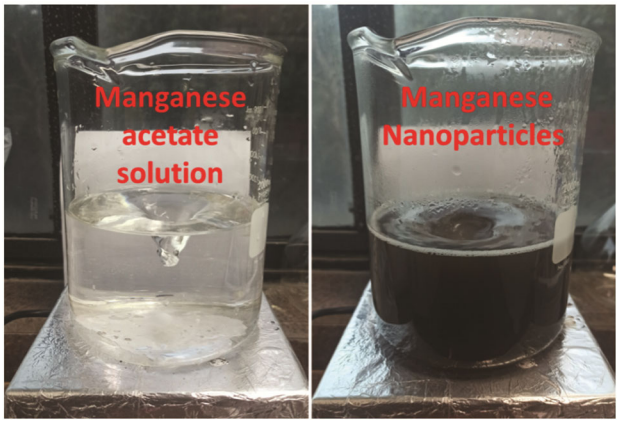


Fig. 1 — Manganese nanoparticles (NPs) formation

3 Materials Characterization

3.1 Structural properties (X-ray diffraction studies)

An X-ray diffraction study of manganese oxide nanoparticles was carried out using BRUKER D8 (Germany) advanced model X-ray diffraction with $CuK\alpha_1$ (λ=1.54056 Å) radiation in the 2θ range 20^0-80^0. The specimen's scanning speed was maintained at 0.50 m/min. The X-rays were detected using a fast-counting detector based on silicon strip technology (Bruker Lynx Eye detector).

The XRD analysis was done before and after calcination. No peaks were sensible in the diagram plotted for manganese oxide before calcination. The XRD was repeated after the calcination of manganese oxide nanoparticles at 600 °C for 2 hours. The 2θ peak was observed at 28.74°, 37.460°,41.28°, 42.3°, 47.35°, 57.6°, and 59.50°, which correspond to (110), (101), (200), (111), (210), (211), and (220) lattice planes of reflection, respectively (Fig. 2). The XRD spectrum reveals that the sample is polycrystalline. The obtained particles were confirmed to be manganese oxide using an XRD graph. The structure was observed to be in the pure tetragonal phase. All major diffraction peaks for all samples were chosen to

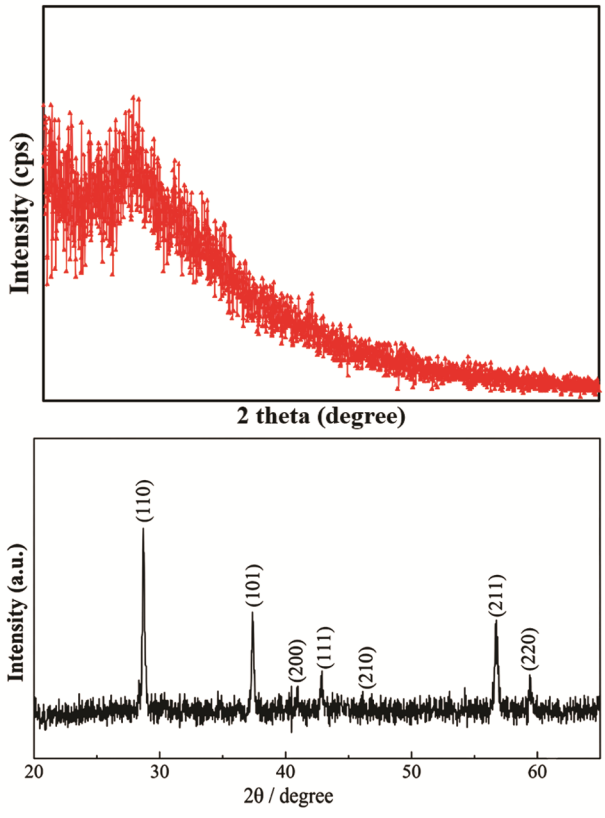


Fig. 2 — XRD diffractogram of manganese oxide nanoparticles

estimate the average size of the nanoparticles using the least squares method. The average grain size was determined using Scherrer's formula and was estimated to be 25.30 nm[16].

The XRD pattern can be indexed as the tetragonal phase of manganese oxide (JCPDS card No. 24-0735) with lattice parameters (a = b = 9.81 and c = 2.84)[17]. Furthermore, no additional diffraction peaks corresponding to impurities were detected, indicating the formation of highly pure and well crystallized manganese oxide nanoparticles.

3.2 Field Emission Scanning Electron Microscope (FE-SEM)

Field emission scanning electron microscopy is a convenient technique to study the microstructure of manganese oxide samples. Scanning electron microscopy and FESEM images were taken to study the surface morphology of cerium (IV) oxide at Hitachi Hi Technologies Corporation, Japan (Model No. S4800).

Figure 3 (a-c) shows FESEM images of manganese oxide calcinated at 600°C with various magnifications. 100 x, 20 K and 50K SEM analyses of the manganese oxide revealed that most particles have a polymorphic morphology. The SEM image shows aggregations with rough, spherical, and arbitrarily oriented particles developed with Lagerstroemia speciosa aqueous extract. Aggregation of nanoparticles arises, possibly due to high surface energy, polarity, and electrostatic attraction[18]. A superior adsorption performance for dye elimination was predictable because of their smaller size and increased surface area[19]. In addition, the size reduction can be attributed to the capping action of the active organic compounds in the extract, which limits particle growth[20].

The size of nanoparticles varies from 83 nm to 400 nm. They consist of some voids that can be used to dope up an additional material to improve their structure.

The crystallite size calculated from the XRD data using Scherrer's equation was 25.30 nm, whereas the particle dimensions observed by FESEM were in the range of 83–400 nm. This difference is attributable to the different length scales measured by the two techniques. The Scherrer equation estimates the average size of coherently diffracting crystalline domains, while FESEM provides the morphological dimensions of individual particles or aggregated particle assemblies. Since the XRD pattern indicates that the synthesized MnO_2 is polycrystalline and the

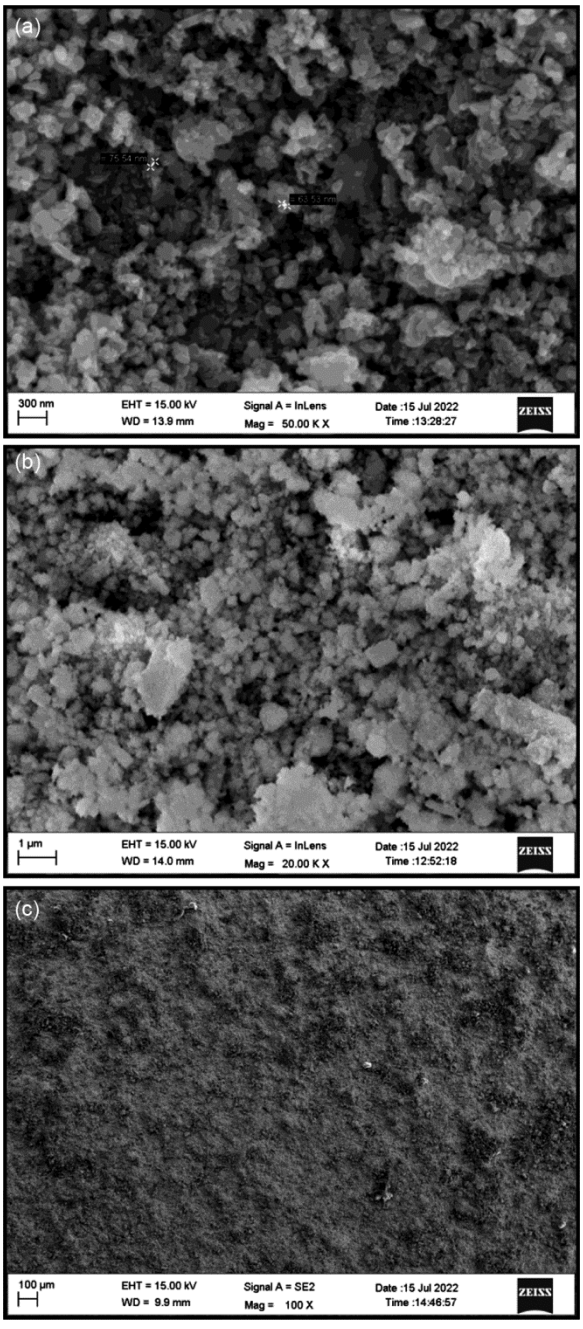


Fig. 3 (a-c) — Field emission scanning electron microscope (FE-SEM) of manganese nanoparticles

FESEM images reveal pronounced aggregation, the larger FESEM dimensions are reasonably attributed to secondary particles formed by the association of multiple smaller crystallites. Thus, the FESEM visible particles of 83–400 nm may comprise several primary MnO_2 crystallites having an average coherent crystallite size of approximately 25.30 nm. The observed aggregation may arise from the high surface

energy, polarity, and electrostatic interactions among the nanoparticles. Therefore, the XRD and FESEM results are complementary and do not represent contradictory particle size measurements.

3.3 Fourier Transforms Infrared Spectroscopy (FTIR)

Fourier transform infrared spectroscopy (FTIR) is an effective tool to identify the functional groups in the studied material. The modes of vibration of chemical bonds and functional groups in the manganese oxide nanocomposites were analyzed using the FTIR spectrum. Figure 4 shows the FTIR spectrum of manganese oxide, which is recorded in the spectral range of 4000–400 cm^{-1}.

The peak at 579 cm^{-1}, credited to the Mn-O bond, appears and turns out to be more and more intense[21, 22]. The immense absorption band at 579 cm^{-1}can be attributed to the Mn-O stretching mode, signifying an O-Mn-O bond in the MnO_2 structure[23]. The peak at wave number 1032 cm^{-1} is attributed to the O-H bending vibrations coupled with Mn atoms, whereas the absorption peak at 1416 cm^{-1} was ascribed to the C-N of the amine. The peak near 1557 cm^{-1} is attributed to the bipedal nitrate[24]. The peaks observed at 2324 cm^{-1}, 2829 cm^{-1}, 2943 cm^{-1}, and 3745 cm^{-1} were ascribed to the stretching vibration bands of C-OH, C≡C, C-H, and −OH, respectively[25–27]. In the aqueous leaf extract, these functional groups may originate from many biomolecules, such as flavones, alkaloids, etc., which can function as reducing and capping agents[28, 29].

3.4 Thermo Gravimetric Analysis

Thermo gravimetric and derivative analysis (TGA/DTA) curves of the prepared manganese oxide nanoparticles were determined and are presented in Fig. 5 (a, b). The heating process was started at room temperature and then increased up to 850 ^{0}C along

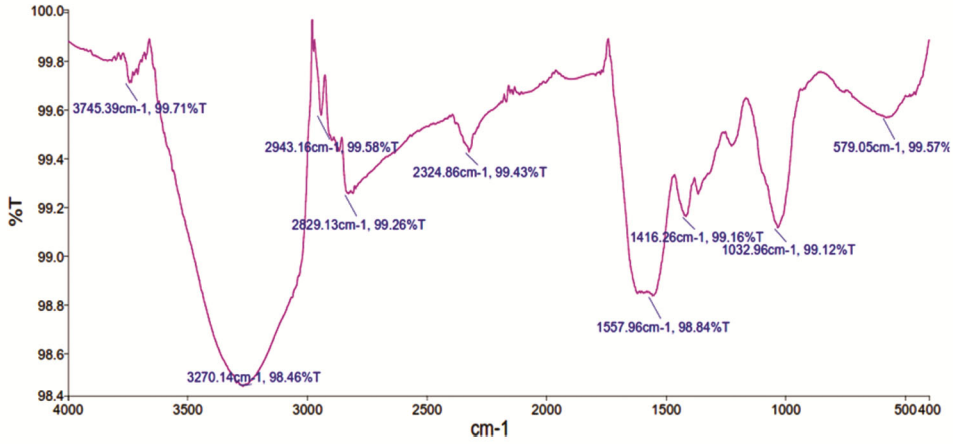


Fig. 4 — FTIR spectrum of manganese oxide nanoparticles

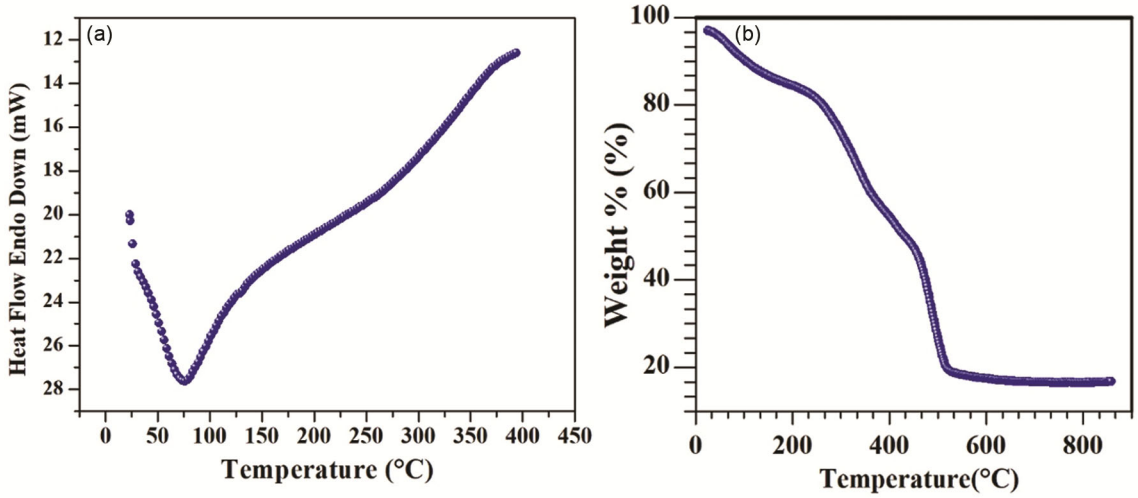


Fig. 5 (a-b) — Thermo gravimetric and derivative analysis (TGA/DTA) curves of the manganese oxide nanoparticles

with a temperature rate change of 10 ^{0}C/min. The first weight loss between 20 and 100 ^{0}C is an initial mass loss attributable to the loss of hydrated water and the water of crystallization since gradual dehydration of manganese oxide takes place in this temperature range. The second stage appears at 100 - 260 ^{0}C, with slight mass loss attributed to the crystallinity and release of unreacted biomolecules present in the sample originating from the aqueous leaf extract. Most compounds decompose at 300 - 320 ^{0}C for a total mass loss of 65–69 %. Stable compounds with higher thermal stability can be attributable to increased ionic and lattice ordering. It has been further noticed that altering of metal ions, charge, shape, or type of functional group appears at 455 - 750 ^{0}C due to the release of coating molecules from the surface of the synthesized α-MnO2 nanoparticles[30]. The total mass loss of the sample is 69 %. No weight loss between 550 and 850 ^{o}C was detected on the TGA curve, which indicates the configuration of MnO_2 nanoparticles as a stable product[31].

According to the DTA curve, the endothermic peak was observed owing to the melting process in the range of 455 ^{0}C, attributed to the material's nano-crystallinity. A broad peak was also obtained at 600 ^{0}C, which is due to the transition from α-MnO_2 to another polymorph of MnO_2.

$$Mn(CH_3COO)_2\,2H_2O \longrightarrow Mn_3O_4 + 4\,CO_2 + C_8H_{18} + 6H_2O\uparrow$$
$$Mn_3O_4 + 4\,CO_2 + C_8H_{18} \longrightarrow Mn_3O_4 + C_8H_{18} + 4\,CO_2 + \uparrow$$
$$Mn_3O_4 + C_8H_{18} \longrightarrow C_8H_{18}\uparrow$$
$$Mn_3O_4 \longrightarrow 3\,MnO + 1/2\,O_2\uparrow$$

4 Optical Properties by UV-Visible Spectroscopy

UV-Visible absorption spectroscopy was employed to investigate the optical properties of the biosynthesized MnO_2 nanoparticles. The absorption spectrum recorded at room temperature is presented in Fig. 6. The spectrum exhibits a pronounced absorption band centered at approximately 365 nm, confirming the formation of MnO_2 nanostructures. The observed absorption feature is associated with charge transfer transitions and the optical excitation characteristics of nanoscale manganese oxide particles. The position and intensity of the absorption band are influenced by several factors, including particle size, crystallinity, surface defects, oxygen vacancies, and quantum confinement effects.

To evaluate the optical band gap energy, the Tauc relation was employed;

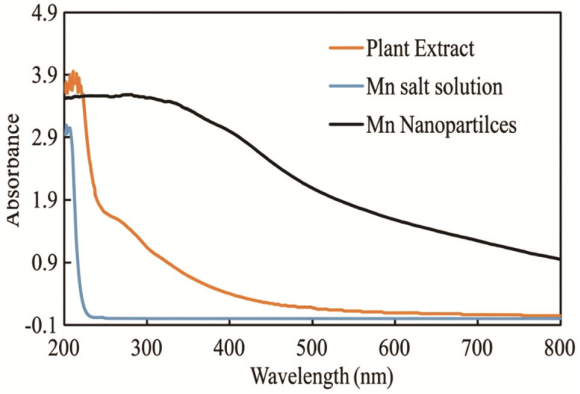


Fig. 6 — UV-Vis spectra of plant extract, Mn solution, and biosynthesized Mn nanoparticles

$$(\alpha h\nu)^2 = A\,(h\nu - E_g) \quad \ldots (1)$$

where α is the absorption coefficient, hν is the photon energy, A is a proportionality constant, E_g is the optical band-gap energy, and n = 2 was used for the direct allowed electronic transition of MnO_2. The Tauc plot was obtained by plotting $(\alpha h\nu)^2$ as a function of photon energy $(h\nu)$, as illustrated in Fig. 6. The optical band gap energy was estimated by extrapolating the linear portion of the curve to the photon-energy axis at $(\alpha h\nu)^2 = 0$.

The extrapolated Tauc plot yielded an optical band gap value of 3.39 eV. The calculated band gap reveals that the prepared nanocomposite can be used as an excellent catalyst in photocatalytic processes.

5 Application of Mn Nanoparticles

All the dye decolorization experiments were carried out by adding Mn NPs (~10 mg) to a solution mixture containing 10 mL of the dye solution having a concentration of 25 mg/L and 1 mL of 3×10^{-2} mol/L $NaBH_4$ solution in screw-cap vials. Then, these mixtures of respective dyes were thoroughly mixed and exposed to direct sunlight (solar radiation). The UV-visible spectra of this reaction mixture were recorded at regular intervals for 0-60 min until the dye solution was decolorized.

To investigate the photocatalytic activity of the as-prepared manganese oxide, the decolorization of the two dyes methyl orange and bromocresol green in an aqueous solution under solar irradiation was examined. Figure 7 reveals that the prepared manganese oxide catalyzes the process efficiently. When dyes are exposed to the prepared manganese oxide and sunlight, the diminishing of pollutant concentration begins. The photocatalytic efficiency is calculated via following Eq.[16];

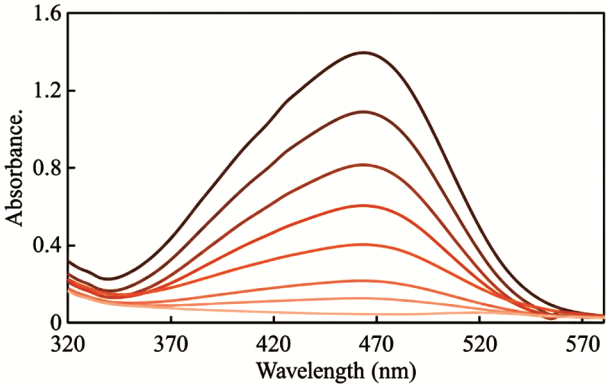


Fig. 7 — UV-visible absorbance spectrum of methyl orange & MnO_2 NPs reaction mixture

$$colorremoval(\%) = \left(C_0 - {}^{C_t}/_{C_0}\right) x\ 100 \quad \ldots (2)$$

where C_0 (mg L^{-1}) is the initial concentration of methyl orange and bromocresol green in solution, and C_t (mg L^{-1}) is the concentration at any irradiation time (min). The photo catalyst process was performed for 60 minutes. The photocatalytic activity was calculated at neutral pH, with about 90 % and 93 % decolorization for methyl orange and bromocresol green, respectively.

Excitation can be enforced to arise through light via light energy (hv) that is equivalent to or more prominent than the band gap energy (Eg) of the semiconductor. Upon irradiation, electrons in the valence band (VB) are excited to the conduction band (CB), generating photo generated electron hole pairs. Subsequently, the electron vacancy or holes were observed to stay in the VB, resulting in an electron-hole pair. These pairs are conveyed to the photocatalytic surface, while O and OH radicals are induced by the overreaction of electron and hole pairs via O_2 and H_2O molecules, respectively.

Photocatalytic studies encompass the idea that manganese oxide NPs can be an effective contender for photocatalytic applications due to their excellent photocatalytic activity[18]. The plot of $\ln(A_0/A_t)$ versus irradiation time exhibits a linear relationship for all samples, indicating that the degradation of the dyes by manganese oxide nanoparticles follows pseudo first order reaction kinetics. (Fig. 8-10). The rate constants of decomposition of MO and BCG were estimated as 0.020 and 0.026 per minute, respectively.

The photolytic degradation of MO and BCG via $NaBH_4$ results in the formation of amino compounds from the azo groups of MO and BCG. The degradation reaction was completed within 60 minutes, as evidenced by the almost zero absorption at 460 nm, as shown in the fig. 7, 9. Thus, the photolytic degradation of MO and BCG by means of $NaBH_4$ in the absence of MnO_2-NPs was thermodynamically favorable but not kinetically. Thus the MnO_2-NPs catalyst supplies an alternative route of low activation energy for the photolytic degradation of MO, which reduces the kinetic barrier, making it thermodynamically and kinetically favorable.

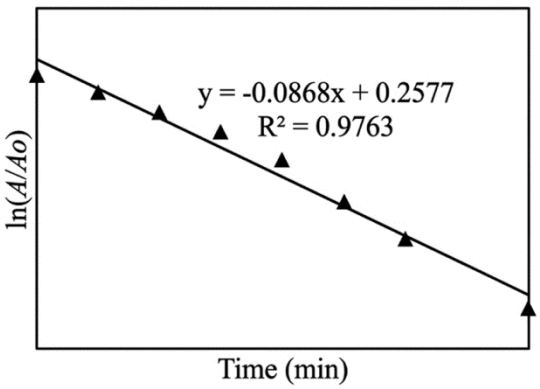


Fig. 8 — Calibration curve Ln (A_t/A_0) vs time

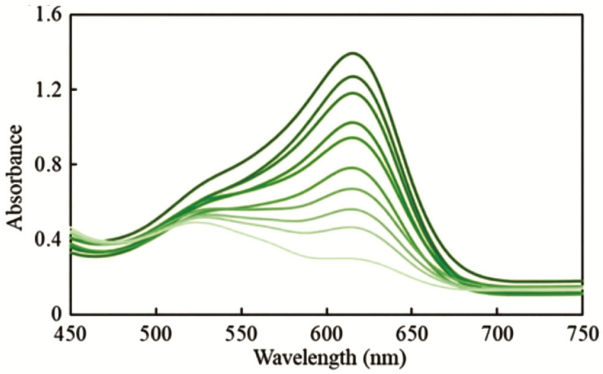


Fig. 9 — UV-visible absorbance spectrum of bromocresol green & MnO_2 NPs reaction mixture

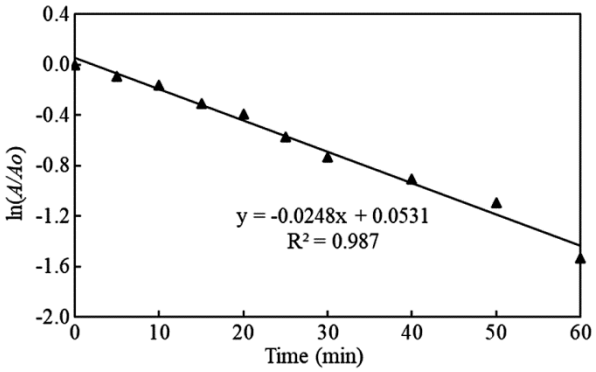


Fig. 10 — Calibration curve Ln (A_t/A_0) vs time

5.1 Mechanism of Dye Removal

The dye removal experiments were performed using the synthesized manganese oxide nanoparticles in the presence of $NaBH_4$ under solar irradiation. Because $NaBH_4$ is a strong reducing agent, the observed dye removal cannot be attributed exclusively to conventional photocatalytic oxidation. Under the experimental conditions employed, $NaBH_4$ provides electrons for the reduction of dye molecules, while the manganese oxide nanoparticles act as a catalyst to facilitate electron transfer between BH_4^- and the dye molecules. Solar irradiation may additionally influence the electronic properties and surface activity of the catalyst; however, its specific contribution to the overall dye removal process cannot be independently established from the present experimental results.

In this process, BH_4^- functions as the electron donor, whereas the dye molecules serve as electron acceptors. The manganese oxide nanoparticles provide active surface sites that facilitate electron transfer from the reducing species to the adsorbed dye molecules, thereby promoting the reduction of the dye molecules[18]. The nanoscale dimensions and high surface area of the synthesized manganese oxide nanoparticles may provide a greater number of accessible active sites, contributing to the observed dye removal efficiency.

The linear relationship obtained from the plot of $\ln(A_0/A_t)$ versus irradiation time indicates that the dye removal process follows pseudo first order kinetics under the experimental conditions. The observed efficiencies therefore demonstrate the catalytic effectiveness of the synthesized manganese oxide nanoparticles in the presence of $NaBH_4$ under solar irradiation.

Accordingly, the process investigated in the present study is more appropriately described as manganese oxide nanoparticle assisted catalytic reduction of dyes using $NaBH_4$ under solar irradiation**,** rather than as an exclusively photocatalytic oxidation process. Since separate control experiments and radical scavenging studies were not performed, the individual contributions of $NaBH_4$ mediated reduction, manganese oxide catalysis, and solar irradiation cannot be quantitatively distinguished. Further control experiments, including dye + $NaBH_4$ without catalyst, dye + manganese oxide without $NaBH_4$ under dark conditions, and dye + manganese oxide under solar irradiation in the absence of $NaBH_4$, would be required to establish the relative contribution of each pathway.

5.1.1 Control Experiments and Mechanistic Considerations

To distinguish the individual contributions of solar irradiation, $NaBH_4$, and MnO_2 nanoparticles to the dye removal process, appropriate control experiments are required. These include (i) dye solution under solar irradiation in the absence of $NaBH_4$ and MnO_2 nanoparticles to evaluate direct photolysis, (ii) dye solution containing $NaBH_4$ under solar irradiation in the absence of MnO_2 nanoparticles to determine the contribution of $NaBH_4$ mediated reduction, and (iii) dye solution containing MnO_2 nanoparticles and $NaBH_4$ in the dark to evaluate the catalytic reduction process in the absence of light.

Since these control experiments were not performed in the present study, the individual contributions of photolysis, $NaBH_4$ mediated reduction, MnO_2 assisted catalytic reduction, and solar irradiation cannot be quantitatively distinguished. Therefore, the observed dye removal is not attributed exclusively to photocatalytic oxidation. Under the experimental conditions employed, $NaBH_4$ acts as a reducing agent, while MnO_2 nanoparticles may facilitate electron transfer between BH_4^- and the dye molecules. Solar irradiation may further influence the surface and electronic properties of the catalyst; however, its specific contribution cannot be established from the available experimental data.

Accordingly, the dye removal results obtained in this study are interpreted as the combined response of the MnO_2 - $NaBH_4$ system under solar irradiation. The observed linear relationship between $\ln(A_0/A_t)$ and irradiation time indicates pseudo first order kinetics under the experimental conditions. Further investigations incorporating the above mentioned control experiments are required to quantitatively establish the respective contributions of photolysis, chemical reduction, catalytic reduction, and light irradiation.

i. Methyl Orange (MO)
ii. Bromocresol green (BCG)

6 Conclusion

The current study discusses the synthesis and characterization of MnO_2 nanoparticles based on the ratio between manganese precursors and *Lagerstroemia speciosa* used as stabilizing agents. The XRD spectrum reveals that the sample is polycrystalline. The structure was observed to be in the pure tetragonal phase. The average grain size was determined using Scherrer's formula and was estimated to be 25.30 nm. The FESEM shows aggregations with rough, spherical, and arbitrarily

oriented particles developed with *Lagerstroemia speciosa* aqueous extract. Aggregation of nanoparticles arises, possibly due to high surface energy, polarity, and electrostatic attraction. A superior adsorption performance for dye elimination was predictable because of their smaller size and increased surface area. The size of nanoparticles varies from 83 nm to 400 nm. The room-temperature UV absorption spectrum shows a prominent excitation band at 365 nm, which corresponds to the MnO_2 nanostructures because of the transition. A band gap is found to be 3.39 eV. The calculated band gap reveals that the prepared nanocomposite can be used as an excellent catalyst in photocatalytic processes. The reaction of degradation of dye was completed within 60 minutes, as evident by the almost zero absorption at 460 nm.

References

1 Sakthi G & Saravana kumari P, *Int Multidiscipl Education Res*, 10 (4) (2021) 112.
2 Siddique M, Fayaz N & Saeed M*, Phys Rev B Condens Matter*, 602 (2021) 412504.
3 Jayandran M, Muhamed Haneefa M & Balasubramanian V, *J Appl Pharm Sci*, 5 (12) (2015) 105.
4 Chen H J, Tian W & Ding W, *Adsorpt Sci & Technol*, 36 (3) (2018) 1100.
5 Sagadevan S, *J Mater Sci & Eng*, 4 (3) (2015) 1.
6 Feng L, Xuan Z, Zhao H, Bai Y, Guo J & Su CW, *Nanoscale Res Lett*, 9 (290) (2014) 1.
7 Mitra S, Pak Y, Alaal N, Hedhili M N, Almalawi D R, Alwadai N, Loganathan K, Kumarasan Y, Lim N, Jung G Y & Roqan I S, *Adv Opt Mater*, 7 (21) (2019) 1900801.
8 Najafpour M M & Allakhverdiev S I, *Int J Hydrogen Energy*, 37 (2012) 8753.
9 Zhang H T, Chen X H, Zhang J H, Wang G Y, Zhang S Y, Long Y Z, Chen Z J & Wang N L, *J Cryst Growth*, 280 (1) (2005) 292.
10 Shu-yan Q, Jing F & Jun Y, *Chin J Nonferrous Met*, 18 (2008) 113.
11 Lu H, Zhang X, Khan A, Li W & Wan L, *Front Microbio*, 12 (2021) 761084.
12 Shaker K S & Abdalsalm A H, *Eng Technol J*, 36 (2018) 946.
13 Majani S S, Sathyan S, Manoj M V, Vinod N, Pradeep S, Shivamallu C & Venkatachalaiah K N, Kollur S P, *Curr Res Green Sustain Chem*, 6 (2023) 100367.
14 Cauerhff A & Castro G R, *Electr J Biotechnol,* 16 (3) (2013) 1.
15 Ingale A G & Chaudhari A N, *J Nanomed Nanotechol,* 2 (2013) 1.
16 Shaker K, AbdAlsalm A, *Eng Technol J,* 36 (9) (2018) 946.
17 Ullah A K M A, Haque M M, Akter M, Hossain A, Hosen M M, Kibria A K M F, Khan M N I & Khan K A, *Mater Res Express*, 7 (2020) 015088.
18 Madhumitha G, Fowsiya J, Gupta N, Kumar A & Singh M, *J Phys Chem Solids,* 127 (2019) 43.
19 Hasan I M A, Salman H M A & Hafez O M, *Environ Sci Pollution Res*, 30 (2023) 28144.
20 Dessie Y, Tadesse S & Eswaramoorthy R, *Arab J Chem*, 13 (2020) 6472.
21 Karnchanawong S & Limpiteeprakan P, *Waste Manage*, 29 (2) (2009) 550.
22 Xará S M, Delgado J N, Almeida M F & Costa C A V, *Waste Manage*, 29 (7) (2009) 2121,
23 Mylarappa M, Lakshmi V V, Mahesh K R V, Nagaswarupa H P & Raghavendra N, *IOP Conf Ser: Mater Sci Eng*, 149 (2016) 012178.
24 Zia J, Aazam E & Riaz U, *Environ Sci Pollution Res*, 27 (19) (2020) 24173.
25 Hoseinpour V, Souri M, Ghaemi N, *Micro & Nano Lett*, 13 (11) (2018) 1560.
26 Prasad K S & Patra A, *Green Process Synthes*, 6 (2017) 549.
27 Mamun M A A, Noor M, Ullah A K M A, Hossain M S, Matin M A, Islam F & Hakim M A, *Mater Res Express*, 6 (1) (2018) 016102.
28 Bystrom A & Bystrom A M, *Acta Cryst*, 3 (1950) 146.
29 Moeen M, Nouren S, Zaib M, Bibi I, Kausar A & Sultan M, *J Taibah Univ Sci*, 16 (1) (2022) 1075.
30 Martin Joseph A & Thilak Kumar R, *Mater Res Express*, 5 (1) (2018) 014002.
31 Zhang Y X, Zhu S, Dong M, Liu C P & Wen Z Q, *Int J Electrochem Sci*, 8 (2) (2013) 2407